On the assimilation of climatological data by means of numerical circulation models, examplified for the Mediterranean Sea

Mediterranean Sea
Numerical modelling
Climatic data
Circulation

Mer Méditerranée
Modélisation numérique
Données climatiques
Circulation

Emil V. STANEV [a], **Hans J. FRIEDRICH** [b]

[a] Department of Meteorology and Geophysics, University of Sofia, 5, A. Ivanov Boulevard, 1126 Sofia, Bulgaria.

[b] Institute of Oceanography, University of Hamburg, Troplowitz Strasse 7, 2000 Hamburg 54, Germany.

Received 6/6/90, in revised form 8/11/90, accepted 27/11/90.

ABSTRACT

Based on Levitus' (1982) data set, a combination of robust diagnostic and fully prognostic techniques is used to evaluate for the Mediterranean Sea a climatology consistent with the physics of the GFDL-OGCM. Model experiments are carried out with 28 levels and with a horizontal resolution of $\Delta\lambda = 1/3°$, $\Delta\varphi = 1/4°$. The model is forced mechanically by wind stress taken from Hellerman and Rosenstein's (1983) data. Sea surface temperature and salinity are prescribed from Levitus' (1982) data. Exchange flows in the Strait of Gibraltar are explicitly prescribed with $1.5 \times 10^6\,m^3\,s^{-1}$.

The focus is put on the analysis of initial and boundary conditions data. The dynamical effects of the exchange flows in the Strait of Gibraltar, as well as the effects of the deep water anomalies are examined. Simulated data are compared with the initial ones and with some other hydrological data. At the most, model adjusted salinities and temperatures depart from Levitus' initial data by 0.02 and 0.05°C in deep layers and by 0.1 and 1°C in the pycnocline. The simulated circulation is generally cyclonic. Velocity profiles reveal a subsurface jet at about 50 m advecting Atlantic water eastwards. With increasing depth a reversal of zonal flow is simulated with a core at about 300 m advecting Levantine Intermediate Water westwards. Assuming homogeneous deep water is a very crude approach to remove physically inconsistent data. The baroclinicity of the deep water proves to be of paramount importance for the model circulation. An adequate assimilation by the model thus seems to be particularly necessary for deep water data.

Oceanologica Acta, 1991, **14**, 2, 97-114.

RÉSUMÉ

Sur l'assimilation des données climatiques par des modèles numériques de circulation. Application à la Mer Méditerranée

Basée sur les données de Levitus (1982), une combinaison de techniques diagnostiques robustes et de techniques pronostiques est utilisée pour évaluer une climatologie de la Méditerranée consistente avec les processus physiques du GFDL-OGCM. Des simulations avec 28 niveaux et une résolution horizontale de $\Delta\lambda = 1/3°$, $\Delta\Phi = 1/4°$, sont effectuées. Le modèle est forcé mécaniquement par la tension de vent reprise dans les données d'Hellerman et Rosenstein (1983). La température de surface de la mer et la salinité sont prescrites d'après les données de Levitus (1982). La valeur prescrite des débits dans le détroit de Gibraltar est de $1{,}5 . 10^6\,m^3\,s^{-1}$.

L'accent est mis sur l'analyse des conditions initiales et des conditions aux frontières. Les effets dus au débit dans le détroit de Gibraltar et aux anomalies des eaux profondes sont examinés. Les résultats des simulations sont comparés avec les données initiales et d'autres données hydrologiques. Les écarts maximaux entre les salinités et les températures calculées et les valeurs initiales de Levitus sont de 0,02 et 0,05°C dans les couches profondes et de 0,1 et 1°C à la pycnocline. La circulation simulée est généralement cyclonique. Les profils de vitesses révèlent, à environ 50 m sous la

surface, un jet qui advecte de l' « eau atlantique » vers l'Est. A plus grande profondeur, dans une couche située à 300 m, l'inversion du courant zonal est simulée, d'où l'advection d'« eau levantine intermédiaire » vers l'Ouest. L'hypothèse d'homogénéité des eaux profondes pour écarter les données physiquement inconsistentes est très grossière. Le caractère barocline des eaux profondes s'avère d'une importance capitale pour les modèles de circulation. Une assimilation adéquate par le modèle semble donc particulièrement nécessaire pour les données en eaux profondes.

Oceanologica Acta, 1991, **14**, 2, 97-114.

INTRODUCTION

In recent years, the Mediterranean Sea has increasingly stimulated the interest and efforts of the scientific community Several international projects have been launched to intensify the oceanographic investigations of the Mediterranean Sea, as for example WMCE (West Mediterranean Circulation Experiment, La Violette, 1985), POEM (Physical Oceanography of the Eastern Mediterranean, POEM Steering Committee, 1985), PRIMO (Programme de Recherche International en Méditerranée Occidentale, IOC, 1989) and others. The interest stems in part from increasing environmental problems, but in addition, this semi-enclosed sea is considered to be an adequate substitute basin for tests of various physical concepts, which should apply to circulation models of the world ocean too. At present, existing models of the Mediterranean Sea are not developed enough to give reliable estimates of such important processes as for example the seasonal variability of deep water formation.

In fully prognostic models (models that can in principle be used to predict ocean currents) driven by climatic atmospheric forcing the model climate tends to drift away from the observed climate. This drift is commonly attributed to deficiencies of the model with respect to the parameterization of unresolved physical processes. On the other hand, circulation patterns produced by strictly diagnostic models (models that use equation of motion and continuity to compute currents directly from density measurement and wind stress field, Sarkisyan, 1975) turned out to be extremely sensitive to inconsistencies in the input data. In principle, a certain mismatch between the atmospheric forcing and the hydrological data seems to be inevitable.

In view of these problems and in view of the general scarcity of data an intermediate class of models has been suggested. The semi-diagnostic approach (Sarkisyan and Demin, 1983) allows the adjustment of an observed hydrological data set subject to physical model constrants by integrating the model for a certain time, t_i. This time interval is chosen with a certain arbitrariness according to the smoothness of the predicted stratification, but it is usually long enough to allow the adjustment of current patterns to density fields. Alternatively, the robust diagnostic approach of Sarmiento and Bryan (1982) introduces Newtonian damping terms into the prognostic equations for salinity and temperature. These terms keep the solution of the model close to the initial values. The integration time t_i and the time constant t_N of Newtonian restoring terms represent the degree of corrections to initial data. With $t_N \to 0$ or $t_i \to 0$ the models approach the fully diagnostic case. With $t_N \to \infty$ or $t_i \to \infty$ the models approach the fully prognostic case. With increasing t_N or t_i the solution depends more an more on the driving forces and model parameters. By selective choice of the time constants a stronger weight may be given to those initial data which seem to be more reliable. This intermediate class of models may in fact help to eliminate physically inconsistent data from a given data set.

Here we adopt the robust-diagnostic concept to assess the quality of a climatic hydrological data set for the Mediterranean Sea. Specifically, the initialization of our model is based on Levitus' (1982) climatological data set for the world ocean, which is available for 33 standard levels on a horizontal resolution of 1°. Levitus analyzed historical data archived up to the beginning of 1978 at the NODC in Washington. The analyzed data set conceals a severe bias in the original data in favour of certain seasons and regions and a serious shortage of observations particularly in the deep ocean. A comparison of his analyzed data with his original profile data for the Mediterranean Sea leads to the conclusion that certain conspicuous inconsistencies in the regularly spaced climatic data are explainable as consequences of an extreme scarcity of deep data in the original observations and of the specific analysis method used to fill the empty spaces: information had to be passed over long distances, and in particular across submarine ridges, which in nature effectively decouple the deep water masses of the basins at both sides.

With the comparison between annual mean climate data and the data simulated by several numerical experiments we want to demonstrate the capacity of the circulation model to eliminate or at least to reduce inconsistencies of the initial data without destroying the more realistic patterns. We start with a short review of general ideas about the circulation in the Mediterranean Sea. Then we briefly discuss the model. The formulation of the experiments is finally followed by a discussion of model climate.

REVIEW OF THE CIRCULATION IN THE MEDITERRANEAN SEA

The Mediterranean Sea is a classical example for a semi-enclosed sea of the concentration type. According to recent estimates, evaporation exceeds total pre-

cipitation and runoff by an average rate of $0.76 \times 10^{11}\,cm^3\,s^{-1}$ (Bethoux, 1979). Salt and mass losses are compensated by exchange flows with the Atlantic Ocean in the Strait of Gilbraltar. Atlantic Water (AW) enters the Mediterranean Sea in the upper layer which has a depth of the order 0 (100 m). The outflow of Mediterranean Water into the Atlantic is a mixture of Intermediate Water (IW) and Deep Water (DW).

As already claimed by Nielsen, the exchange flows in the Strait of Gibraltar affect the circulation throughout the Mediterranean Sea (Nielsen, 1912). His map of surface currents in Figure 1 *a* reveals the eastward current along the North African coast as the most prominent large scale feature. Although Schott argued in favour of the generally cyclonic wind field as the main driving mechanism, his map of surface currents in Figure 1 *b* looks quite similar to Nielsen's map (Schott, 1915). Both current patterns show cyclonic gyres in the separate basins. This sense of rotation is consistent with the vortex forcing by the wind. There is one conspicuous difference between the two maps: in Sirte Bay Schott's circulation is anticyclonic in contrast to Nielsen's, but this anticyclone is a feature which is also supported by the more recent map presented in Figure 1 *c* (Ovchinnikov *et al.*, 1976). The last current map is based on dynamical computations using more than 10 000 hydrological station data obtained between

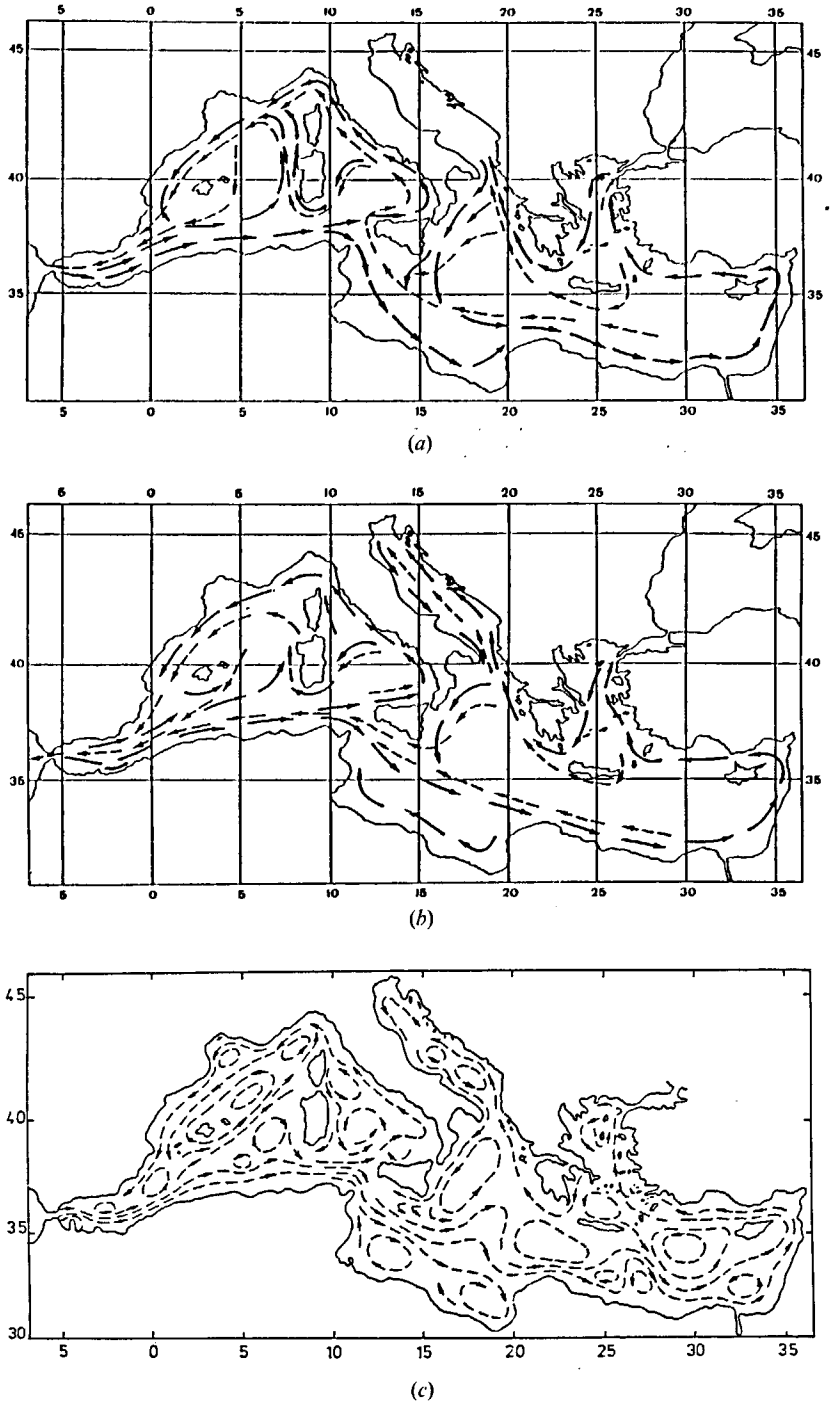

Figure 1
Surface currents: a) from Nielsen (1912); *b) from Schott* (1915); *c) from Ovchinnikov* et al. (1976).

1880 and 1969. Most of these data (4000) are from the summer months July, August, September, and furthermore, most of them have been observed in the Western Basin. This sampling bias makes it difficult to estimate the reliability of the current map. The difficulty is enhanced by the sensitivity of the dynamical method to the choice of adequate reference levels. A constant level at 1000 m was chosen for the computation of the dynamical surface topography balancing the current pattern of Figure 1 *c*.

The eastward current along the North African coast carries AW far into the eastern basin, where it is still traceable by its surface or sub-surface salinity minimum. The sub-surface minimum is particularly apparent in summer, when heating and strong evaporation establish a warm and saline surface layer. The quasi-zonal section of salinity profiles along the current, shown in Figure 2 *a* (taken from Ovchinnikov *et al.*, 1976), illustrates the rapid adjustment of AW to Mediterranean conditions by mixing with local water masses and by exchange processes with the atmosphere.

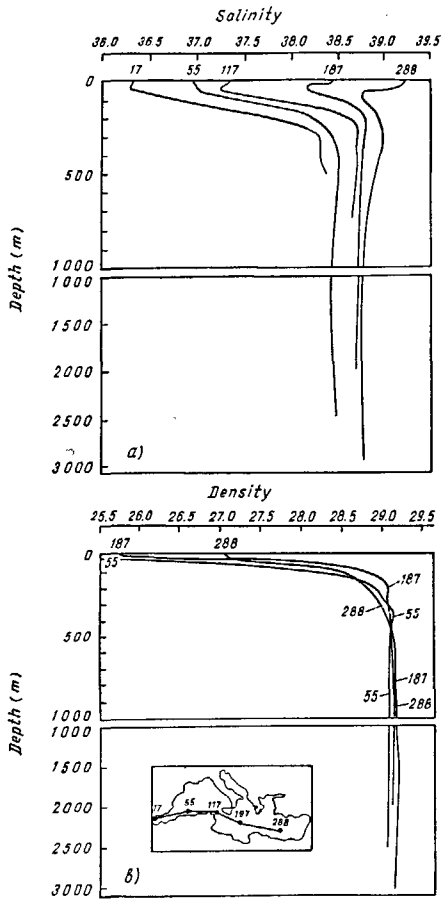

Figure 2

a) Vertical salinity profiles in summer; b) Vertical density profiles in summer (from Ovchinnikov et al., 1976).

Figure 2 *b* shows density profiles along the same section. Obviously, the upper layer containing AW is practically decoupled in summer from the intermediate layer below by a strong vertical density gradient of 2-3 σ_θ-units per 100 m. The intermediate layer is continuous from its main source area in the Levantine Sea of the eastern basin to the Strait of Gibraltar. The Levantine Intermediate Water (LIW) is observed as a distinct salinity maximum. This water mass has been extensively studied for example by the core method (Wüst, 1960). LIW is formed in the Levantine basin during winter, when the surface layer has been sufficiently cooled, and strong, dry winds blow frequently over the-eastern basin.

Currents in the LIW-layer, computed dynamically with a reference level at 1000 m, are generally too small to clearly separate westward advection from noise. This probably is another consequence again of the insufficient data coverage, because hydrographic data from the western basin usually show a distinct reversal of current directions between AW and LIW layers.

Below intermediate layers, *i.e.* below 600 m approximately, the Mediterranean Deep Water (DW) forms a remarkably homogeneous water mass of high oxygen content. Small but significant differences are observed in salinities and temperatures of DW between the Western and the eastern basins. There seems to be no direct exchange of deep water across the sill in the Strait of Sicily (Plakhin, 1971; 1972). The high oxygen content of DW is of course typical for a concentration basin. During winter, deep convection in limited areas intermittently ventilates the deep layers. The Gulf of Lions south of France is the most conspicuous deep water source in the western basin. Surface cooling in the Adriatic Sea dominates deep water formation in the eastern basin..

The three layer structure of the large scale circulation in the Mediterranean Sea, as crudely outlined above, is basically contained and supported in Levitus' coarse climatic data set. Figure 3 depicts a salinity section of his data from the Strait of Gibraltar through the Strait of Sicily all the way to the Levantine coast. The section

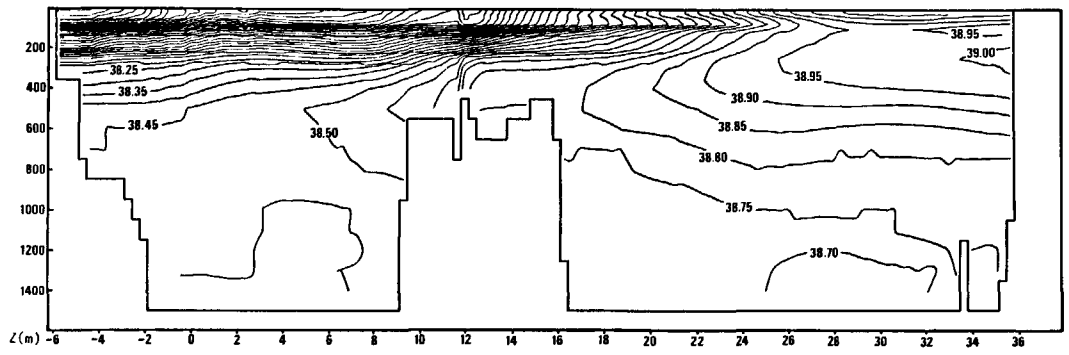

Figure 3

Vertical salinity cross-section along the dotted line shown in Figure 4.

clearly shows for instance the LIW-core. In detail, however, this large scale pattern seems to be modified by an intensive meso-scale eddy field, which recently attracted strong attention (Millot, 1987; Robinson *et al.*, 1987). *In situ* and remotely sensed data as well as model results show strong baroclinic eddies persisting for a long time at specific locations. Topographic control presumably prevents the exchange of eddies between the sub-basins. Some individual eddies are quasistagnant and may be considered as a semi-permanent feature of the general circulation.

MODELLING THE CIRCULATION OF THE MEDITERRANEAN SEA

At present, several groups are developing numerical models of the Mediterranean Sea or of its sub-domains. A special symposium was devoted to this topic during the XIV General Assembly of the European Geophysical Society. Among the model concepts presented, there were process studies (*e.g.* Heburn, 1989; Madec *et al.*, 1989), as well as general circulation experiments (*e.g.* Stanev and Friedrich, 1989 and Pinardi and Navarra, 1989). Basically there are two categories of models: Some apply an inverse modelling technique (*e.g.* Tziperman and Hecht, 1988); others make use of primitive equations and apply the freely available OGCM developed at the GFDL in Princeton (*e.g.* Stanev and Friedrich, 1989 and Pinardi and Navarra, 1989). There is an increasing interest in modelling the main sub-domains, *e.g.* Malanotte-Rizzoli and Bergamasco (1989; 1990) for the eastern basin and Beckers (1990) for the western basin.

Formulation of the Model

Here we follow the second approach, and we continue with experiments done previously on a coarser grid (Stanev *et al.*, 1989). We use the GFDL model in the version coded by Semtner (1974). This model applies the Boussinesq approximation and hydrostatic conditions. A rigid lid assumption filters fast moving surface gravity waves. The formulation of the model has been widely published. For further details we refer the reader to the original texts (Bryan, 1969; Semtner, 1974).

Figure 4 shows the coastline and selected isobaths of our model topography. The horizontal resolution is $\Delta\lambda = 1/3°$ and $\Delta\varphi = 1/4°$. For the latitude of the Mediterranean Sea, both these steps correspond to approximately 28 km on the spherical coordinate grid of the model. Islands smaller than a meshsize are neglected by the model. A total of six islands is resolved, Rhodes Island being the smallest with an area of one grid cell. The Strait of Messina is too narrow to be resolved by the grid. There is no volume transport through this strait and in this sense Sicily is not an island. Diffusive fluxes of heat and salt are nevertheless predicted by the model in the Messina Strait. Computations are carried out at 28 levels. Details for the vertical structure of the model are given in the fourth section. Some of the levels in the model differ from Levitus' standard levels. At these levels the initial stratification was obtained by linear interpolation. Linear interpolation was also applied horizontally to specify the initial stratification on the fine grid from Levitus' 1°-data set.

Our data assimilation experiments are based on the robust diagnostic method suggested by Sarmiento and Bryan (Sarmiento and Bryan, 1982); that is, in the prognostic equations for salinity and temperature we introduce Newtonian damping terms:

$$(1)\quad T_t + \mathbf{v}.\nabla T + w T_z = F^T + \gamma (T^C - T)$$

$$(2)\quad S_t + \mathbf{v}.\nabla S + w S_z = F^S + \gamma (S^C - S).$$

Here the horizontal velocity vector and the vertical velocity component are denoted as $\mathbf{v}$ and w respectively. The last term on the right hand side of (1) and (2) tends to restore the solution towards the climatic initial data S^C and T^C with time scales $t_N = 1/\gamma$. In their transport model for the North Atlantic Sarmiento and Bryan use γ as an exponential function of depth:

$$(3)\quad \gamma(z) = 1/t_D + (1/t_S - 1/t_D)\exp(-z/h),$$

where t_S and t_D are surface and deep values of t_N, and h is a penetration depth. For our γ-profile we adapt the parameters of the standard case of Sarmiento and Bryan (1982); *i.e.* $t_S = 50$, $t_N = 250$ days, and $h = 500$ m.

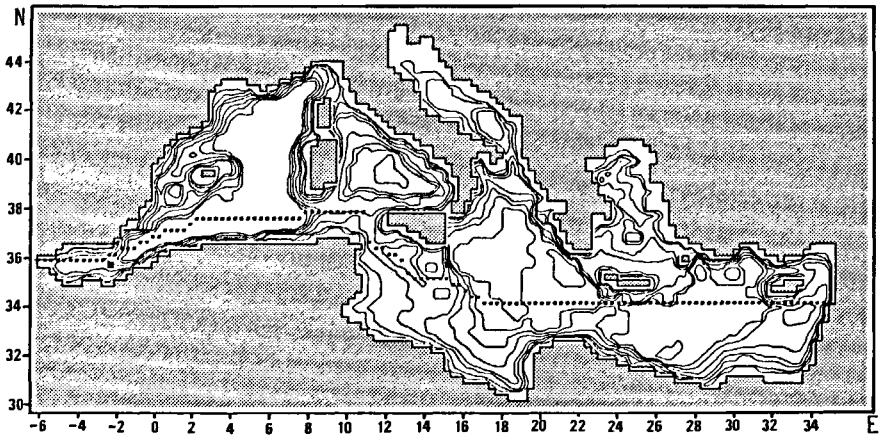

Figure 4

Bottom topography used in the numerical model. This map has horizontal resolution of $\Delta\lambda = 1/3°$ *and* $\Delta\varphi = 1/4°$, *and the following isobaths are plotted:* 50, 100, 250, 1 000, 1 500, 2 000, 3 000, 4 000 *m. Vertical profiles given in Figure* 6 *are plotted in the points marked by dark squares. The dotted line marks the position of the cross-section plotted in Figure* 3.

In some of the experiments free adjustment in selected layers with $\gamma=0$ will be allowed too.

The method is robust in the sense that it does not have the extreme sensitivity to the temperature and salinity input fields of the classical diagnostic model. It is similar to the four-dimensional analysis used in meteorology to assimilate data which are received randomly in time and space. In the present study, as in Sarmiento and Bryan (1982) all observations are combined to form the time averaged fields T^C and S^C. This approach is a consequence of the small amount of data that are available for assimilation in the traditional sense, particularly in the Mediterranean Sea. It can be regarded as a tool to analyze climatic data.

The exponential decrease in γ is chosen to account qualitatively for the decrease of velocity and property gradients with depth, and to maintain approximately a constant ratio between the scales of advection and restoring. As compared to the experiments of Sarmiento and Bryan with their North Atlantic model the use of their standard γ profile implies a ratio on our finer grid which is one order of magnitude larger. Even with a thermohaline scale velocity, V*, of $1\,\mathrm{cm\,s^{-1}}$ horizontal advection dominates over Newtonian damping in the evolution of salinity- and temperature-fields. Estimating the age of AW in the Levantine Sea from the salt budget gives a range of 1.5 to $4.5\,\mathrm{cm\,s^{-1}}$ or the advecting velocity (Lacombe *et al.*, 1981).

Important physical processes remain in the subgrid scale. The eddies in the MEDOC area, for instance, have diameters of order 0 (10 km). They are assumed to contribute to the process of the deep water formation, Madec *et al.* (1989). These and other processes scaling with the baroclinic Rossby radius have to be parameterized in the model. Here we use the traditional concept of eddy exchange coefficients. The eddy diffusion terms of (1) and (2) are modeled by:

$$(4)\quad F^T = A_{TH} a^{-2} \nabla^2 T + \left(\frac{A_{TV}}{\delta} T_z\right)_z$$

$$(5)\quad F^S = A_{TH} a^{-2} \nabla^2 S + \left(\frac{A_{TV}}{\delta} S_z\right)_z$$

The same constant values of the coefficients are taken for the two "tracers" salinity and temperature. The vertical eddy diffusivity, A_{TV} is parameterized as a function of vertical stability in terms of a Richardson Number R_i predicted locally by the model:

$$(6)\quad A_{TV} = \frac{A_{MV}}{1+\alpha R_i} + A_B$$

For neutral stability, $R_i=0$, vertical diffusivity is the sum of vertical eddy viscosity A_{MV} and a background diffusivity A_B, which retains small vertical diffuse fluxes in case of a strong vertical stability. This parameterization has been successfully introduced in the GFDL-OGCM for experiments with tropical ocean models (Pacanovski and Philander, 1981).

The value of δ in (4) and (5) parameterizes convection in the model. It equals 1 in case of neutral or stable stratification; formally, $\delta=0$ describes the algorithm for instantaneous convective adjustment of unstable sections in the water column. This heat and salt conserving adjustment is also a standard procedure in the GFDL-OGCM.

Model values for the diffusivity coefficients A_{TH} and A_B as well as for eddy viscosities A_{MH} and A_{MV} have been determined experimentally, searching by try and error for the smallest values consistent with the stability of model solutions. All our experiments have been carried out with the following set of parameters:

$$A_{MV}=10^{-3},\quad A_{MH}=5\times10^{3},\quad A_{TH}=10^{2},\quad A_B=10^{-5};$$

all units are $\mathrm{m^2\,s^{-1}}$.

With these values the Munk lateral boundary layer is sufficiently resolved, and the Peclet number is large enough to prevent diffusive fluxes from dominating advection.

Boundary conditions

The set of equations is completed with the continuity equation and with the momentum equations of the standard GFDL-OGCM. Adequate boundary conditions are required to solve the circulation model. At the sea surface, $z=0$, at the bottom, $z=-H(\lambda, \varphi)$, and at solid lateral boundaries we use the following conditions:

$$(7)\quad w=0,\qquad \rho_0 A_{MV} v_z = \tau,$$
$$(S, T)=(S^C, T^C)\quad \text{at } z=0$$

$$(8)\quad w=-\mathbf{v}.\nabla H,\qquad v_z=0,$$
$$(S_z, T_z)=(0,0)\quad \text{at } z=-H$$

$$(9)\quad \mathbf{v}=0,\qquad \mathbf{n}.\nabla(S, T)=0$$

at lateral walls.

All the symbols have their standard meanings. Thus, at the surface we apply the rigid lid condition, a momentum flux proportional to the wind stress τ and a Dirichlet condition to fix the salinity and temperature data at their climatic values. At the bottom we apply the kinematic and free slip conditions and exclude normal fluxes of salt and heat. The latter condition is also applied at lateral walls together with a no slip condition for the horizontal momentum equations.

In contrast to previous experiments, where the Strait of Gibraltar was kept closed in the model (Stanev *et al.*, 1989), we now want to study in particular how the exchange flows in the strait affect the interior circulation. We assume that the net transport through the strait is zero. From budget considerations it is known that the annual mean in- and outflows are about 20 times larger than the net inflow, and the zero transport condition should not critically falsify the simulated currents in the interior. Note also that for salinity and temperature at sea surface we use (7) rather then prescribed fluxes, thus no net water flux is allowed in the model at the sea surface as well.

According to observations in the strait, the flow direction closely correlates with the density anomaly: light AW enters the Mediterranean Sea, and heavy MW spills out across the sill into the North Atlantic (Farmer and Armi, 1989). In spite of the highly nonlinear dynamics of this process we simply assume the zonal current velocity at the open boundary to be propor-

tional to a fixed density anomaly. With the present horizontal resolution the condition involves one velocity profile only. In our boundary condition:

(10) $u = -b(\rho - \bar{\rho}^G)$,

where

$$\bar{\rho}^G = 1/H_G \int_0^{H_G} \rho \, dz,$$

and H_G is the depth of the strait.

We chose the proportionality constant b in such a way that

$$\int_{(y)}\int_0^h u \, dy \, dt = -\int_{(y)}\int_h^H u \, dy \, dz = 1.5\,10^6 \, m^3 \, s^{-1},$$

with h given by $\rho(h) = \bar{\rho}^G$.

The transport value of 1.5 Sverdrup is in the range of estimates from observations (Bethoux, 1979; Bryden and Stommel, 1984).

In all our experiments the transports in the Strait of Gibraltar as well as the forcing by sea surface boundary conditions are constant in time and they correspond to annual mean data. The mechanical forcing is taken from wind stress data of Hellerman and Rosenstein (1983). Their 2°-data were linearly interpolated onto the model grid points. Salinity and temperature data for the boundary conditions were similarly obtained from Levitus' (1982) climatic data set. These forcing functions are shown in Figure 5. All three of them are strikingly smooth.

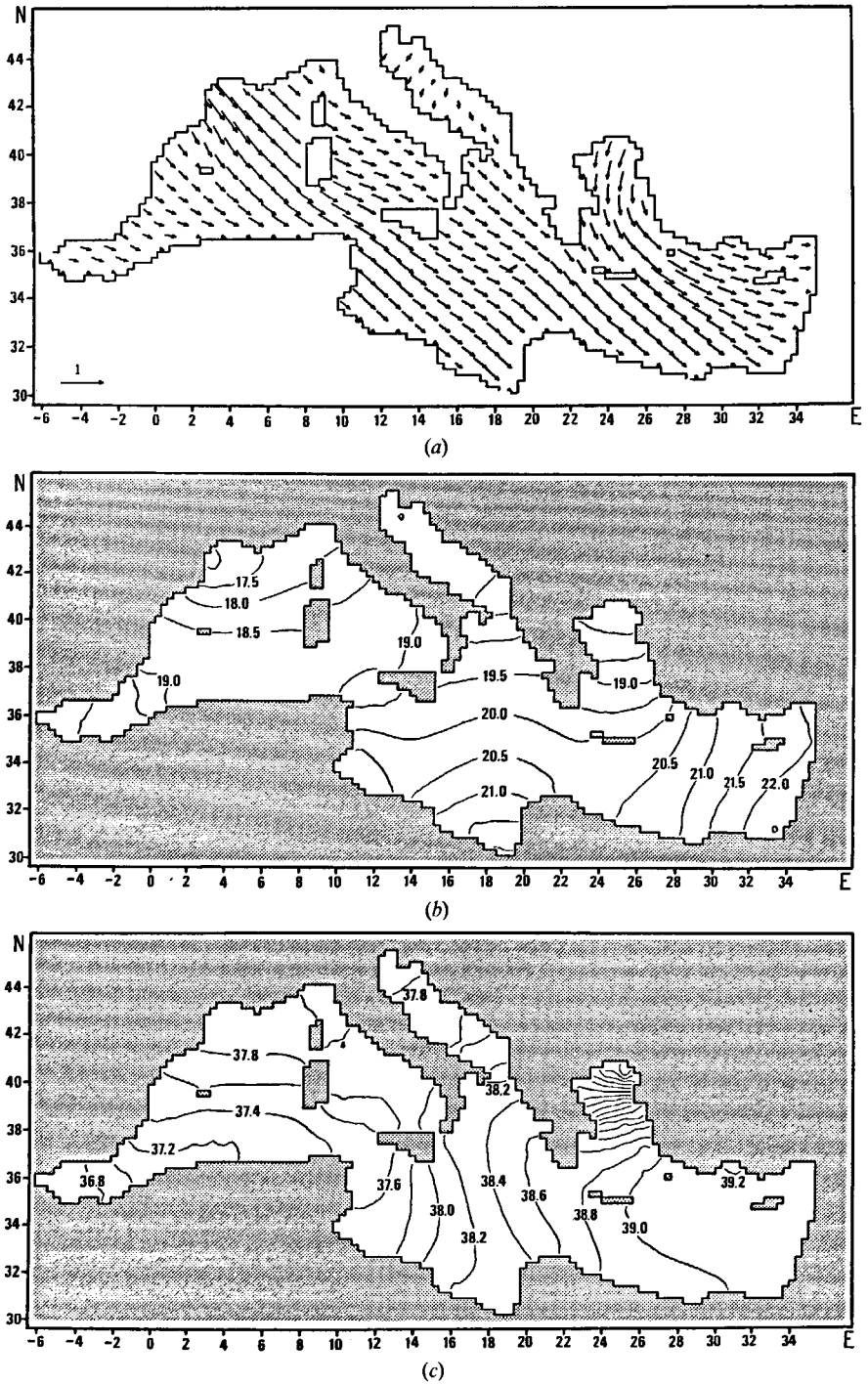

Figure 5

Annual mean wind stress: a), sea surface temperature; b) and salinity; c). The standard arrow length corresponds to wind stress 1 CGS.

The wind stress, Figure 5*a*, is generally directed towards the Southeast. Particularly over the eastern basin, the cyclonic sense of rotation is obvious. The magnitude amounts to 0.75 dynes/cm^2.

Sea surface temperatures, Figure 5*b*, cover a range of about 5°C, with maximum values around 22°C close to the easternmost coastline and minimum values around 17°C off the southern coast of France.

Sea surface salinity, Figure 5*c*, ranges between 0.03916 to the West of Cyprus and 0.03583 in the Aegean Sea. Salinity decreases also towards the northern part of the Adriatic Sea and towards the Strait of Gibraltar, where AW enters with surface values for salinity and temperature of 0.0367 and 18.47°C. Vertical profiles of salinity and temperature at the open boundary in the Strait of Gibraltar are given in Table 1.

The model uses an empirical nonlinear equation of state to compute density from salinity, temperature and pressure. The density of MW is predominantly controlled by salinity. At the surface, the heaviest water is found to the northwest of Rhodes, and the lightest off the Dardanelles. The density range is close to 2 σ_t-units. This is also the differences in potential density between the inflow and the outflow through the Strait of Gibraltar.

NUMERICAL EXPERIMENTS WITH THE MEDITERRANEAN SEA OGCM

A series of five experiments was carried out to study model solutions in response to the forcing with the annual mean climate described in the "Boundary conditions" section. With the exception of the Newtonian damping coefficient γ, the physical parameters of the model were the same in all the five experiments. Initially, the model was started from rest with a stratification deduced from Levitus' annual mean data by linear interpolation. Table 2 contains some information about these initial data and about the vertical structure of the model. In the surface layer the model includes a total of 2572 wet grid cells. The last column of Table 2 shows how the number of wet cells decreases with depth. All our numerical experiments were done on the Siemens 7.882 of the Computer Center at Hamburg University.

Table 1

Annual mean Levitus profiles in Gibraltar strait. For the last two columns see (10).

k	z (*m*)	S	T (°C)	$(\rho-\bar{\rho}^G)/\bar{\rho}^G$	u (cm s^{-1})
1	8	.03670	18.47	−0.005	65.02
2	20	.03671	17.97	−0.004	63.47
3	31	.03674	17.26	−0.004	59.91
4	50	.03678	16.54	−0.004	50.48
5	75	.03693	15.56	−0.003	36.29
6	100	.03715	14.90	−0.002	22.54
7	125	.03737	14.43	−0.001	11.97
8	156	.03757	13.99	0.000	0.15
9	200	.03774	13.67	0.001	−14.09
10	250	.03809	13.29	0.002	−29.50
11	313	.03824	13.19	0.003	−42.90

Table 2

Average stratification of the Mediterranean Sea (according to Levitus' annual mean data set).

		Temperature (°C)			Salinity			Density (σ-units)			wet
k	z (*m*)	Mean	Maximum	Minimum	Mean	Maximum	Minimum	Mean	Maximum	Minimum	%
1	8	19.28	22.04	16.98	38.10	39.16	35.83	27.37	28.05	26.10	100
2	20	19.08	21.79	16.98	38.13	39.15	36.68	27.50	28.17	26.73	100
3	31	18.53	21.29	16.42	38.16	39.12	36.71	27.70	28.37	26.96	100
5	50	17.64	20.65	15.51	38.18	39.08	36.75	28.00	28.68	27,23	99
5	75	16.21	18.94	14.35	38.22	39.03	36.89	28.47	29.06	27.65	99
6	100	15.28	17.57	13.51	38.31	39.00	37.10	28.85	29.36	28.07	98
7	125	14.93	17.09	13.22	38.40	39.01	37.30	29.11	29.55	28.43	97
8	156	14.75	16.82	13.15	38.46	39.01	37.50	29.33	29.70	28.81	96
9	200	14.64	16.61	13.15	38.53	39.01	37.67	29.60	29.90	29.22	94
10	250	14.48	16.13	13.16	38.62	39.01	38.07	29.94	30.16	29.83	92
11	313	14.36	15.74	13.17	38.67	39.00	38.24	30.30	30.47	30.26	89
12	400	14.28	15.16	13.22	38.70	38.97	38.30	30.73	30.87	30.69	87
13	500	14.11	14.71	13.25	38.70	38.91	38.42	31.17	31.33	31.17	82
14	600	13.79	14.35	13.02	38.68	38.88	38.43	31.66	31.86	31.70	78
15	700	13.66	14.18	12.98	38.66	38.87	38.42	32.07	32.27	32.14	72
16	800	13.59	13.96	12.96	38.64	38.83	38.43	32.54	32.70	32.58	70
17	900	13.53	13.88	12.87	38.63	38.83	38.43	33.02	33.15	33.01	66
18	1 000	13.47	13.78	12.91	38.61	38.76	38.42	33.48	33.57	33.44	62
19	1 100	13.44	13.76	12.91	38.61	38.76	38.42	33.85	34.01	33.88	61
20	1 200	13.43	13.74	12.96	38.60	38.76	38.40	34.28	34.44	34.31	56
21	1 300	13.41	13.72	12.96	38.61	38.76	38.41	34.74	34.88	34.75	53
22	1 400	13.38	13.64	12.97	38.60	38.76	38.41	35.21	35.31	35.16	49
23	1 538	13.38	13.64	12.98	38.60	38.77	38.41	35.75	35.91	35.76	47
24	1 750	13.37	13.69	12.94	38.58	38.77	38.40	36.69	36.82	36.67	44
25	2 063	13.38	13.69	12.95	38.58	38.78	38.41	37.98	38.14	38.00	37
26	2 500	13.42	13.73	12.95	38.60	38.78	38.39	39.88	39.99	39.86	27
27	3 000	13.59	13.73	13.16	38.66	38.78	38.45	42.00	42.07	41.95	9
28	3 500	13.70	13.70	13.69	38.65	38.66	38.65	44.04	44.04	44.04	1

Standard deviations of the Levitus' stratification data (not shown in Table 2) emphasize the smoothness of this data set and the approximate homogeneity of the deep layers. For the upper 300 m these values are about 1°C for temperature and between 0.0005 and 0.0008 for salinity. In deep layers the values reduce to 0.3°C and 0.0003. Concealed behind the average values in Table 2, the initial stratification includes a considerable amount of static instabilities, particularly in deep layers. This drawback of the data base in part motivated and determined the design of our experiments. In particular, we separate the upper layers (above 1 400 m), with an initial stratification based upon a reasonable data coverage, from the deep layers (below 1 400 m), where conspicuous gradients suggest a poor quality of initial data.

The numerical experiments which we will discuss below are listed in Table 3. We describe here the specification of the experiments in the text. Four letters are used to define the experiments, that correspond to the specific structure of the model. The first letter is always "E" and means experiment. The second and the third letter denote the type of computations in the upper layer (above 1 400 m) - second letter, and in the deep layer (down to the bottom) - the third letter. "D" denotes diagnostic, "R" denotes experiment with restoring term, "H" water is assumed to be homogeneous, "P" - prognostic computations. For the H-cases, the properties of the deep water mass were fixed at: $S = 0.038700$ and $T = 13.30$°C. At the interface, these values provide a slight stability with respect to the upper layers. The last letter denotes the boundary condition at the Gibraltar Strait, "C" - closed, "O" - open.

Table 3
Summary of model experiments.

	Above 1 400 m	Below 1 400 m	Gibraltar Strait	Reference in text
1	infinite γ	infinite γ	closed	EDDC
2	γ from (3)	homogeneous	open	ERHO
3	γ from (3)	homogeneous	closed	ERHC
4	γ from (3)	$\gamma = 0$	closed	ERPC
5	γ from (3)	$\gamma = 0$	open	ERPO

In experiments ERPC and ERPO temperature and salinity in deep layers below 1 400 m are simulated prognostically ($\gamma = 0$). ERPC is initialized with the simulated salinity, temperature and velocities of ERHC, but the initial temperature and salinity of DW is taken from Levitus data. Since in some locations these data are vertically unstable, the integration initiates strong vertical mixing which could penetrate above 1 500 m. To avoid this process, we fix temperature and salinity in the upper layer equal to ones in E 3 and simulate penetration of the signal from above. Thus, errors in deep layers do not affect the data in the upper 1 400 m, where no vertical instability is observed. After the convection stops the model is integrated further with the restoring terms (3) in the upper layer and with $\gamma = 0$ in deep layers. Thus, the deep water adjusts to the general circulation determined by the forcing and by the vertical structure of water masses in the upper 1 400 m.

The experiments discussed above need less computer time to reach the steady state than the fully prognostic experiments. As the analysis shows, almost no trends of salinity and temperature exist in ERHO and ERHC after integration time of about two-tree times longer then the maximal t_N. Also, if we have free deep layer (ERPC and ERPO), the model's solution convergence towards quasi-equilibrium state is speeded in comparison to the experiments with all levels resolved prognostically.

GENERAL FEATURES OF SIMULATED DATA

Initial vertical temperature and salinity profiles, and the profiles resulting from ERPO are shown in Figure 6 for two grid points. The position of these points is chosen close to the Strait of Gibraltar and to the Strait of Sicily (*see* Fig. 4). Zonal velocity profiles in the same locations are plotted too. Vertical profiles of the simulated data are smoother then the initial ones. In some depths (500 m in the Alboran Sea and 1 500 m in the Ionian Sea) initial data seem to be not correct. For instance, in these points the vertical temperature profiles indicate maximums and minimums, that does not correlate with the salinity distribution and result in unstable stratification. During the integration, some inconsistent features in the vertical stratification are "corrected" by the model. In the deep layers, the simulated temperature and salinity depart from the initial ones with about 0.05 and 0.02°C respectively. In the pycnocline these deviations reach 0.5-1°C and 0.1.

The model simulates realistically subsurface AW that can be detected by the subsurface salinity minimum even in the eastern basin. This simulated minimum does not present in the initial data but corresponds to the observational data, and correlates with the strong eastward advection of subsurface water.

From Figure 6 it can be seen that velocity profiles simulated in ERPO differ substantially from the diagnostically simulated ones (EDDC). This indicates that the model circulation pattern is not severely dominated by the initial data. Due to the inflow of AW, surface currents in the Alboran Sea increase significantly. At about 170 m a reversal of zonal flow is simulated. The core of the western transport of Levantine Intermediate Water (LIW) is at about 300 m. East from both straits velocity profiles reveal subsurface jet at about 50 m advecting AW eastwards. In the Sicily Strait surface currents in ERPO are more than twice stronger than in EDDC.

Qualitative similarity in vertical temperature and salinity profiles in EDDC and ERPO indicates that Newtonean restoring terms keep water mass distribution close to the initial data. This could be expected, since $t_N \ll t_V$, where t_V is the time scale corresponding to vertical (diffusive) processes. However, the hydrological data at the depth of AW and even LIW change substantially due to the fact that t_N is bigger or of the order of simulated atvective time scale. Thus, currents shear is free to adjust to driving forces and to the modified in the model distribution of mass in the upper

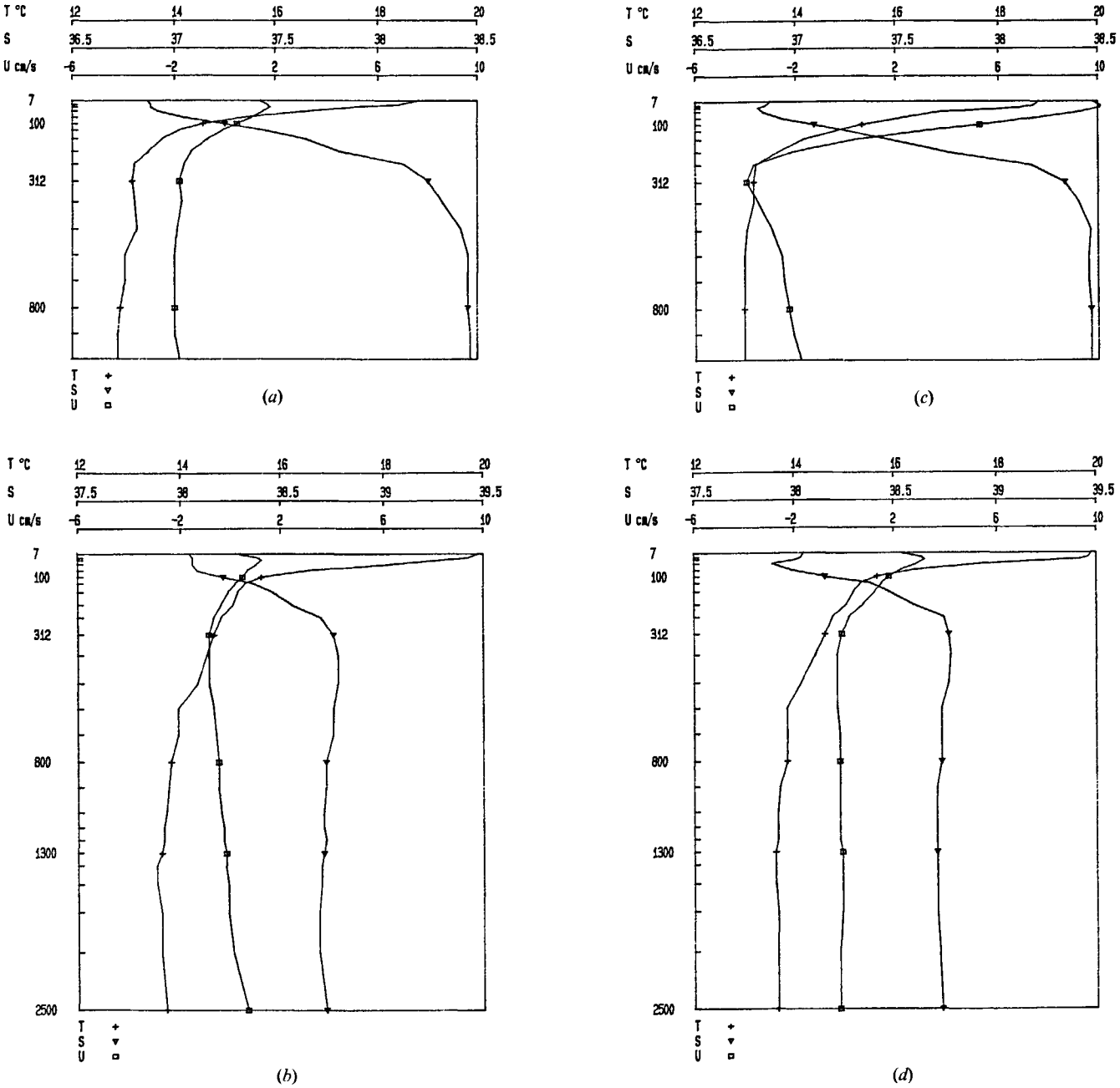

Figure 6

Vertical profiles of temperature, salinity and zonal velocity component in points marked by shaded squares in Figure 4: a) EDDC in th Alboran Sea; b) EDDC east of the Sicily Strait; c) ERPO in the Alboran Sea; d) ERPO east of the Sicily Strait.

1 400 m. Since currents are close to geostrophic, the difference in velocity profiles simulated in EDDC and ERPO indicates that the horizontal distribution of mass has changed substantially. This can be illustrated in Figure 7. Data analysis shows also that there is a good correlation between simulated currents, *see* the "Horizontal circulation" section, and the distribution of temperature and salinity. This manifests that the advection in the model is of primary importance in formation of the horizontal distribution in salinity and temperature.

Simulated in ERPO data can be regarded as synthetic data. They are calculated by the model, that has adjusted some robust features in initial data to driving forces and to the Mediterranean Sea bottom relief. Such kind of restored dynamical systems as the model ERPO can be regarded as a simple tool to assimilate climatic data under some deficit, or bad quality, in certain volumes of model area.

INTEGRATED HORIZONTAL MASS TRANSPORT

Results from the experiments EDDC, ERHO and ERPO are shown in Figure 8. Common feature in these plots is the relatively weak circulation in the western basin compared to the circulation in the eastern one. However, the circulation in the baroclinic model, also in the western basin is much more intense than in a barotropic one (not discussed in this work). The simulated transport in the model driven by wind only

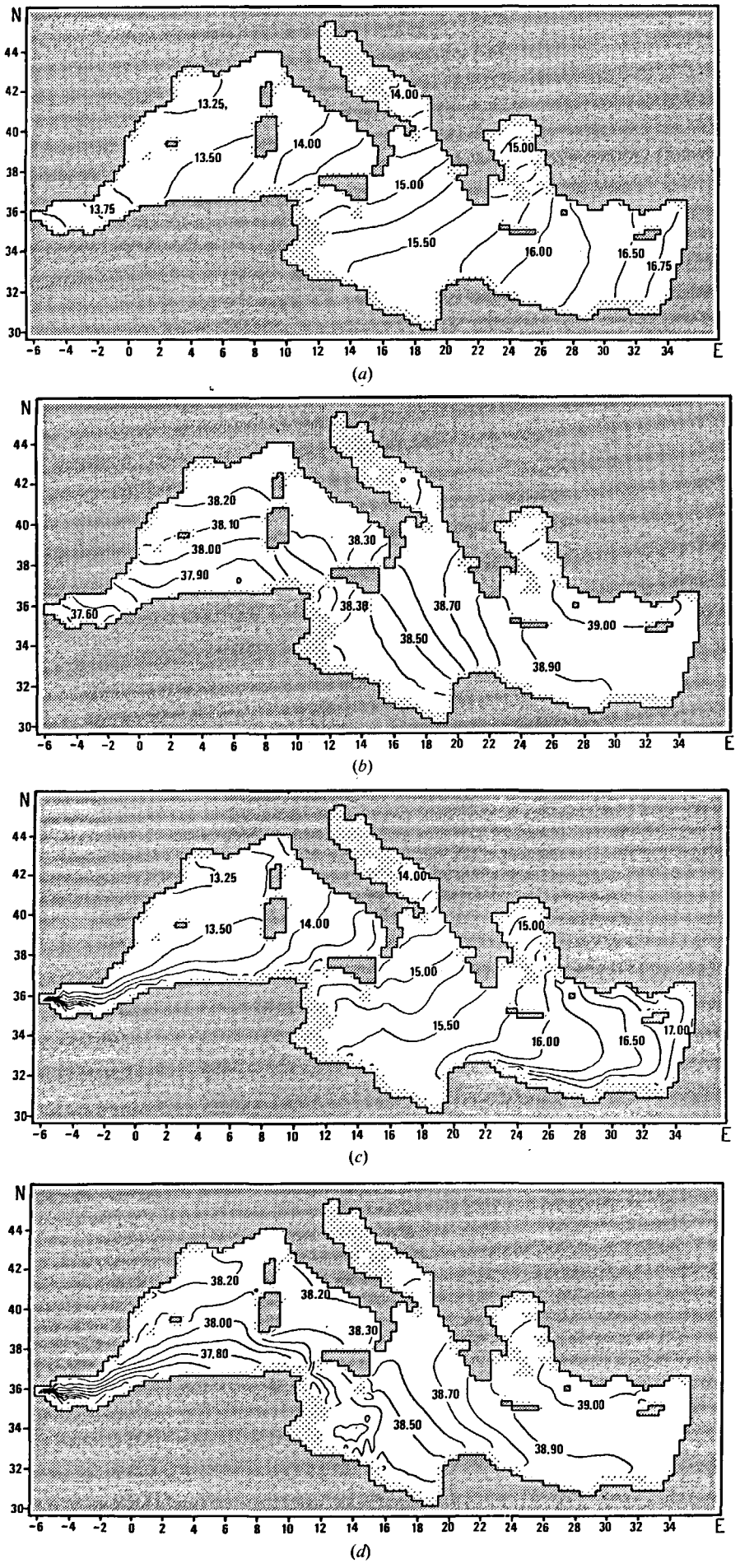

Figure 7
Initial and simulated data at 156 *m. a) initial temperature; b) initial salinity; c) simulated temperature; d) simulated salinity.*

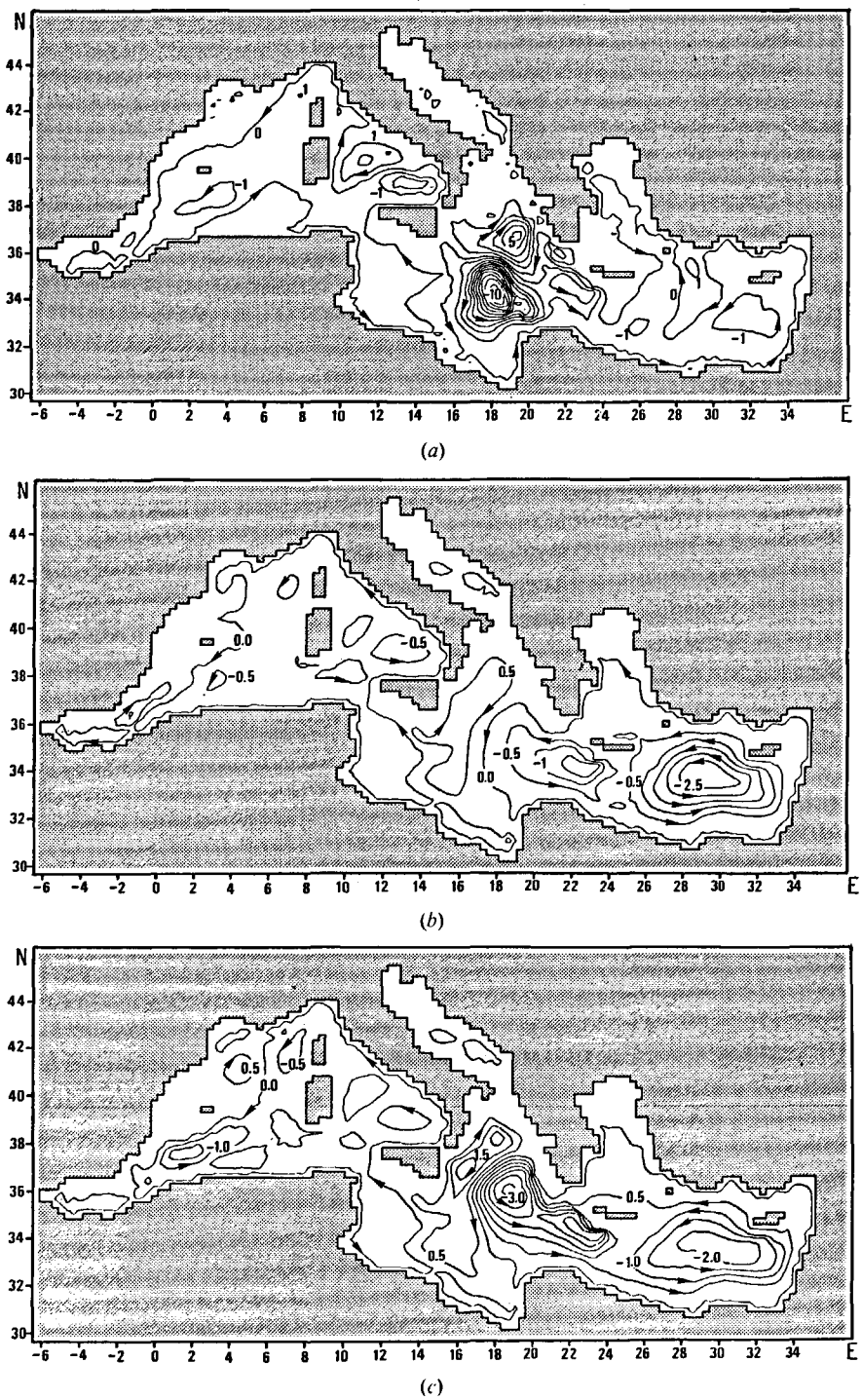

Figure 8
Total mass transport stream function. a) EDDC; b) ERHO; c) ERPO.

reaches: $0.21 \times 10^6 m^3 s^{-1}$ in the western basin; $0.32 \times 10^6 m^3 s^{-1}$ in the Tyrrhenian Sea; about $0.5 \times 10^6 m^3 s^{-1}$ in the Ionian Sea; $0.2\text{-}0.3 \times 10^6 m^3 s^{-1}$ in the Levantine Sea. In the baroclinic experiments the transport increases with an order of magnitude. This, as well as some other numerical results which we will show later, manifests that the determination of the circulation in the Mediterranean Sea should take account primarily to the baroclinicity.

The main feature in the stream function shown in Figure 8 *a* is the intense circulation in the Ionian Sea. Notice that the contour interval in this figure is $10^6 m^3 s^{-1}$, *i.e.* twice larger than in Figure 8 *b*, *c*. The total transport between the centers of the gyre couple (only 300 km) is more than $15 \times 10^6 m^3 s^{-1}$. As was already pointed out, initial data in deep layers in the Ionian Sea seem not to be correct. Water column is vertically unstable in some locations and the horizontal gradients are out of the generally observed ranges. This can contribute to the formation of unrealistic circulation in this area.

Another region with relatively intense circulation simulated in the diagnostic model is the Tyrrhenian Sea. A couple of cyclonic and anticyclonic cells can be seen

with a transport of about 5×10^6 m^3 s^{-1}. As is known, the circulation in this sea is generally cyclonic. However, the diagnostic computations do not reveal such pattern which manifests that the quality of the simulated results is not satisfying. There are at least two approaches to improve the simulated circulation: to prepare new hydrological data set, or to try to "correct" the data in the model. The results of the second approach are shown in Figure 8*b*, *c*.

Figure 8*b* corresponds to ERHO. With homogeneous deep layers below 1 400 m the circulation in the Ionian Sea changes drastically compared to that in EDDC. This indicates that the gyre couple in the Ionian Sea in EDDC results mainly from the specific deep data. There is substantial change of circulation in the entire sea. In the eastern basin, the model simulates generally cyclonic circulation with two cells east and west from the Island of Crete. Eastern cyclonic gyre which is not resolved in the diagnostic model is the most intense gyre in ERHO.

Vertically averaged circulation in the western basin is about twice weaker than in the eastern one. As it will be shown further, in the eastern basin the circulation does not reverse with increasing depth, and the total transport reaches relatively large values. In the western basin there are strong deep compensation currents which tend to decrease the integrated transport. Thus, no pronounced gyre circulation is simulated in this part of the sea. This result seems to confirm the conclusions of Millot (1987), who claims that eddy field dominates the gyre circulation. In our GCM, however, eddies are not resolved, and as a result, the gradients of the stream function are rather weak.

Below we discuss some of the results of ERPO with prognostically simulated deep water. Comparison between Figure 8*b* (ERHO) and Figure 8*c* (ERPO) indicates that baroclinicity of deep water results in substantial change of the integrated mass transport. In ERPO the Ionian cyclonic gyre is more intense than the Levantine one. The transport in the second one decreases by about 25% compared to the transport in ERHO. However the circulation in the Ionian Sea in ERPO is more intense than the circulation in ERHO. Qualitatively, this circulation has some small similarity to the one in EDDC. Thus, we could expect that ERPO simulates Deep Water (DW) characteristics, qualitatively similar to the general characteristics in initial data field. This model data, however, are exposed to the general circulation conditions, and are adjusted to the forcing, bottom topography and the modified initial data in upper 1 400 m. Deep water baroclinicity simulated in ERPO results in some intensification of the circulation in the western basin too. Like in ERHO, however, the vertically integrated transport does not reveal such features as the North African current. Some indications of formation of sub-basin gyres (the closed isolines) can be found in Figure 8*c*.

To simulate the transport around the islands Takano (1974) approach is used in the model. Since ($\psi_{island} \neq 0$), the annual mean transport between different islands, and between islands and the coast ($\psi_{coast} = 0$) can be estimated (Tab. 4). In this table the transport between an island from the vertical column and another one from the horizontal row is directed to the right from the line connecting the first and the second island, provided that the value in the table is positive. It is difficult to compare these values with experimental ones, as there are no such experimental data. Bethoux (1980) suggested that water fluxes across some sections can be calculated using water and salt budgets, as well as observed salinity. There is an agreement between the direction of the transport simulated in the model and calculated by Bethoux (1980). However the magnitude of the model transport is less than the one calculated by Bethoux. This can be explained having in mind that rather smooth annual mean data are used in the model, and probably the insufficient resolution might result in some underestimation of the model simulated transport.

Table 4

Vertically integrated transport in 10^6 cm^3 s^{-1} between some islands and between islands and coast simulated in ERPO.

	Sardnia	Corsica	Crete	Rhodes	Cyprus	Coast
Balcaric	0.27	0.33	0.74	0.32	0.61	0.16
Sardinia		0.06	0.47	0.05	0.34	−0.11
Corsica			0.41	−0.01	0.28	−0.17
Crete				−0.42	−0.13	−0.58
Rhodes					0.29	−0.16
Cyprus						−0.45

The transports simulated in ERHO and ERPO between some islands and the coast does not differ substantially. As the total stream function at the coast is zero, its value in the islands is equal to the transport between the island and the coast. Below we refer to some of these values in 10^6 m^9 s^{-1}: $\psi_{Sardinia} = -0.13$ in ERHO *versus* -0.11 in ERPO, $\psi_{Crete} = -0.50$ in ERHO *versus* -0.58 in ERPO. This comparison demonstrates that the baroclinicity of DW does not change significantly the general mass transport features. However locally, as can be seen from the comparison of Figures 8*b* and 8*c*, the total transport is too sensitive to the DW anomalies.

According to (10), we impose in the Strait of Gibraltar only baroclinic signal, and for the total transport the strait is practically closed. As it can be expected, no severe changes of the total transport result from the change of the boundary condition at the open boundary. If there is no exchange in the strait (ERHC) we have: $\psi_{Sardinia} = -0.09$ and $\psi_{Crete} = -0.49$ in 10^6 m^2 s^{-1}. In the barotropic model driven by wind only, the corresponding values are: $\psi_{Sardinia} = 0.01$ and $\psi_{Crete} = 0.1$. Obviously these values are qualitatively quite unrealistic and too small, that brings us to the conclusion that the baroclinicity, particularly in the upper 1,400 m layer, is the main factor which determines the transport in the Mediterranean Sea.

HORIZONTAL CIRCULATION

Currents at 50 m resulting from the diagnostic model are shown in Figure 9*a*. The main circulation feature is the cyclonic gyre in the Ionian Sea and the weak cyclonic circulation with more intense southern branch

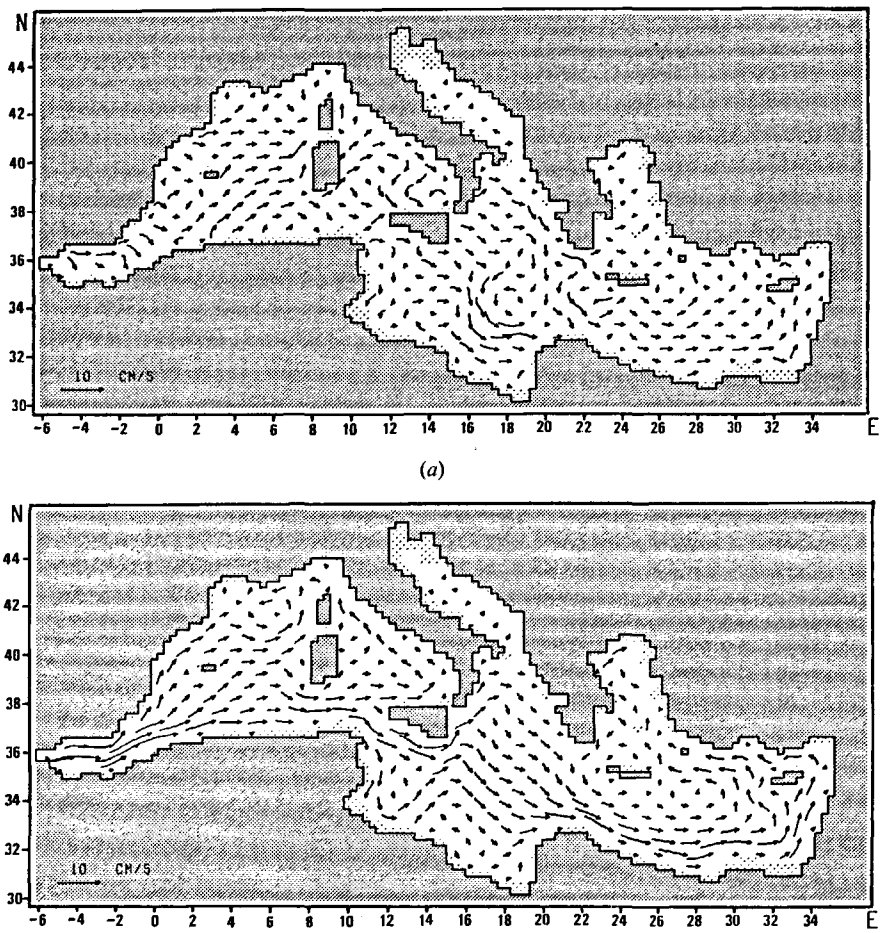

Figure 9
Currents at 50 m in EDDC a), and ERPO b).

in the Levantine Sea. In the eastern basin, currents direction is generally eastward, and no indications of formation of gyre type circulation can be found. No indications of eastward transport of AW through the Strait of Sicily can be seen in Figure 9*a*. There are also some other local inconsistencies in currents pattern, and as a whole they differ substantially from the ones shown in Figure 1. This demonstrates that with Levitus' (1982) data set, the diagnostic model does not simulate realistically the general circulation.

Due to the change of temperature and salinity compared to the initial ones, the circulation in ERHO-ERPO changes drastically. All current patterns at 50 m in the eastern part of the sea are similar to the one shown in Figure 9*b* (ERPO). In the western Mediterranean the baroclinic signal originating in the Strait of Gibraltar results in formation of strong current (magnitude more than 10 cm s^{-1}) entering the Algero-Provencal basin from the Alboran Sea. This flow is split in two branches flowing towards West and North-West. After reaching the latitude of Balearic islands, the northern branch turns towards the African coast. In ERHC and ERPC there is no intense current along the African coast, as the baroclinic transport in the strait is set to zero.

In all experiments ERHO-ERPO the model simulates cyclonic circulation north from the Balearic front, that seems to agree with the general features of circulation in this area, (*see* Fig. 1 *c*). Northward current along the western Corsican coast and the flow coming out from the Corsican channel form the Ligurian current. However, this current is too weak, and does not penetrate along the Catalonian coast. Experiments with barotropic model failed in simulating Ligurian current too. Thus, it seems that the wind forcing in this particular area is not quite correct.

After passing the strait of Sardinia the main flow branches, and the northern branch enters the Tyrrhenian Sea. In ERHC, ERHO, and ERPC the currents in this sea are similar to these in Figure 9*b* (ERPO). This current map is in agreement with the general circulation patterns determined from observations (*see* Millot, 1987). There is no clear indication of any kind of circulation along the eastern Sardinian coast. Most of the water entering the Tyrrhenian Sea flows northward and pass through the Corsican channel.

In the strait of Sicily the surface current forms two branches. The southern one follows the African coast and forms a large loop. To the east from Sicily, approximately after the northern branch passes the Malta bank, both branches merge, and branch again. The southern one flows to south-east as a wide current. No indications of rotating currents in the Ionian Sea as in Figure 9*a* (EDDC) can be found in the results of ERHO-ERPO. In the Levantine Sea, south of the Cyprus, the main current branches again, and the right branch passes inbetween this island and the coast.

Annual mean circulation in the adjacent seas (Aegean and Adriatics) is weak compared to the circulation in the main basins, and has generally cyclonic rotation.

In the western basin the circulation changes strongly between 125 and 200 m. At 156 m, the model ERHO simulates still intense eastward current originating from the Alboran Sea. It was surprising that in the model with free DW (ERPO) no more eastward transport of DW is simulated at 156 m (Fig. 10*a*). This indicates that the baroclinicity of the DW jointly with the effect of the strait contributes to some change of circulation patterns in intermediate depths. In the strait of Sicily, the simulated transport at 156 m correlates with the observed westward transport of LIW. Pronounced anticyclonic gyre is formed at this depth close to the Lybian coast.

Currents simulated in ERPO at 313 m are shown in Figure 10*b*. To the south from Sardinia, LIW forms two branches. The northern one follows Sardinian and Corsican western coast what corresponds to the results of Millot (1987). However, the intense westward current almost below the eastward surface flow (south from the Balearic islands) has not been reported by this author. As he claims, no pronounced vein in the southern part of the western basin is observed in some of the recent hydrological data. According to Millot's results, eddies may play important role in distributing salinity and temperature at the depth of LIW. In our model, however, they are not well resolved, and this might be the explanation of the simulation of well defined westward transport.

The circulation at 313 m in the eastern basin remains qualitatively similar to the pattern in the upper levels. There is a tendency of establishing an anticyclonic gyre extended in the north-south direction (Fig. 10*b*). However, this tendency does not extend to deeper levels. At 600 m, and down to the bottom small anticyclonic circulation cell remains, which is located close to the Italian coast (*see* Fig. 11*b*).

Deep water circulation simulated in ERHO and ERPO is shown in Figure 11. Analysis of model data indicates that the difference between the results of the two experiments increases in deep layers. The best agreement between the two panels of the figure is observed in the Levantine basin, where the circulation is dominated by the westward transport. Weak cyclonic circulation in the Ionian sea (ERHO) intensifies in ERPO, due to the inhomogeneity of the model simulated DW. In the western basin, deep currents originate in the north and has southward direction. This is in agreement with the results of Wüst (1960) who demonstrated that similar transport can be determined from the distribution of oxygen. Again, like in the eastern basin, DW anomalies result in some local differences between deep current patterns (compare Fig. 11*a* with Fig. 11*b*).

The comparison between deep currents resulting from EDDC (not shown here) with the discussed above shows that in the deep levels of the Ionian Sea there is

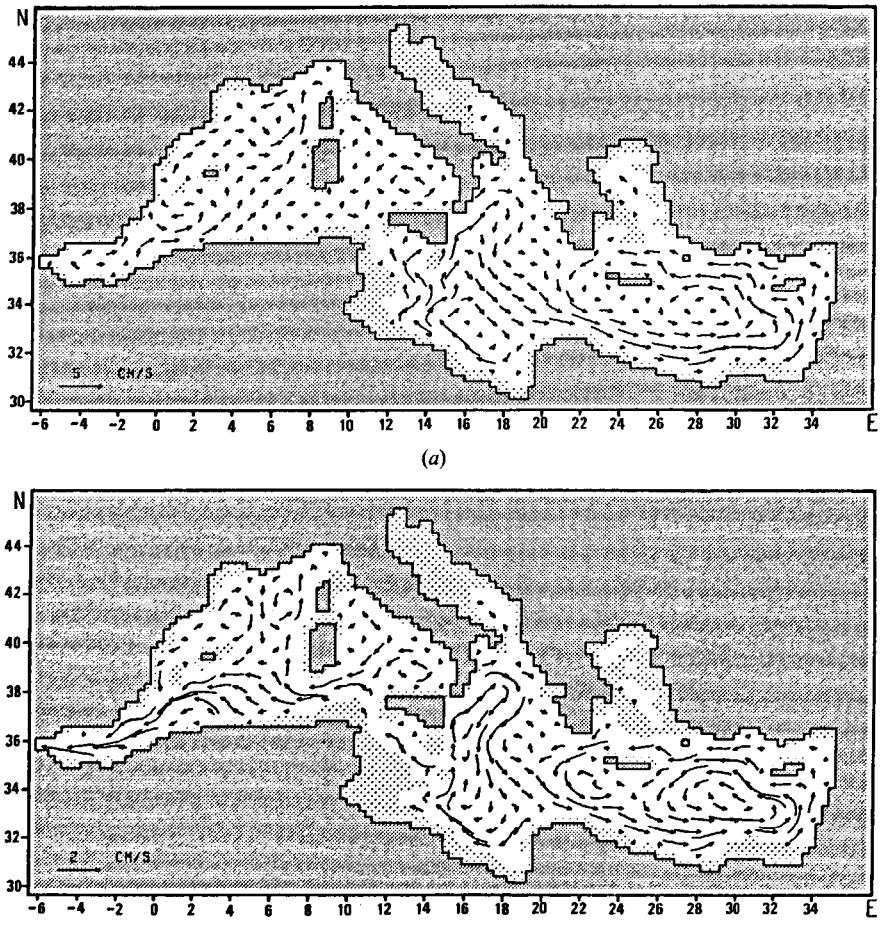

Figure 10
Currents simulated in ERPO at 156 *m a), and* 313 *m b).*

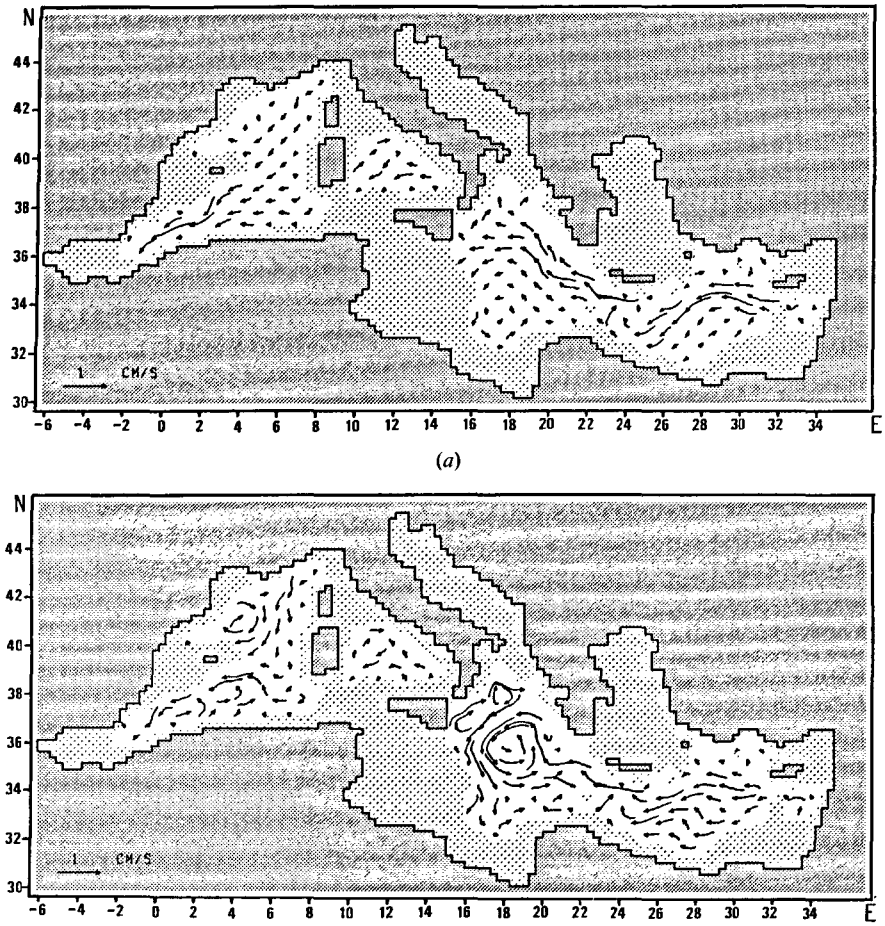

Figure 11
Currents at 1,300 *m. a) in ERHO; b) in ERPO.*

some qualitative similarity between the results of EDDC and ERPO. This indicates that the prognostic calculations below 1 400 m enable us to simulate some features in hydrological fields similar to those in the initial data. However, the simulated data is consistent with the model physics and forcing. Assuming homogeneous DW is very crude approach to remove physically inconsistent data. In some areas, and particularly in deep layers, the circulation is very sensitive to temperature and salinity gradients. Model reconstruction of DW data seems to be a reasonable approach in such water volumes where the data are not reliable.

DISCUSSION

The historical data used to construct the Levitus Atlas shows insufficient data coverage, particularly in deep layers. Since the radius of influence is too large for the Mediterranean Sea, and as no control is done whether the data belong to the same connected area, some errors in the climatic data set are generated. As it has been shown (*see* "Review of the circulation in the Mediterranean Sea") the vertical cross-sections made from the climatic data (Fig. 3) incorporate the main features in water mass distribution: AW, LIW and DW. Vertical profiles (Fig. 6) also indicate agreement with other observational data, compare with Figure 2. However, initial temperature and salinity maps (Fig. 7 *a, b*) are very smooth, and reveal only crudely some large scale features.

One possible approach to determine the Mediterranean Sea circulation using the existing data is proposed in this work. Since the initial data show some errors, for instance instabilities, and since they are not consistent with the model physics and forcing, they have to be "corrected". With the aid of the restoring terms in the equations of salinity and temperature (1,2) chosen to be large enough to keep the general vertical stratification close to the observed one and small enough to allow the model to correct and to adjust the data, we get advantage of the most general and robust information which the initial data contain. If we want to correct horizontal structure of temperature and salinity we should prescribe t_N bigger or of the order of the advection time scale. Choosing t_N to increase with depth corresponds to the fact that time scale increases with depth. Such assumption makes deep layers more flexible to adjust to the circulation characteristics resulting from the distribution of temperature and salinity in upper layers. There is another reason too to increase the inverse time parameter with depth. In the deep layers, the amount of data is generally insufficient to construct reliable data set. From the other side, the ratio between measurements errors and horizontal gradients increases with increasing depth. Thus, DW should be assimilated in the model with special care in

order not to involve erroneous information in the model. In the model area where the data are very "noisy" or unstable it is preferable to carry out fully prognostic computations ($t_N \to \infty$).

As it was shown, the model tends to "correct" the erroneous data, and to produce some new features like the subsurface salinity minimum, that are not presented in the initial data. In the same time it retains the most general physical information from the initial data as the vertical stratification. Thus, we produce synthetic data set. In the deep layers the simulated temperature and salinity depart from the initial ones with about 0.05 and 0.02°C respectively. In the pycnocline these deviations reach 0.5-1 and 0.1°C. The change of the initial data in the model is extremely well pronounced in the surface layer. For instance, the subsurface AW can be detected by the subsurface salinity minimum even in the eastern basin. This corresponds to the observational data, and results from the increased salinity of surface water and the strong eastward advection of subsurface water.

In the nonrestored models the circulation is simulated using boundary conditions only. In the experiments with free deep layers there is a thick "sponge" layer in the upper 1 500 m. In such kind of dynamical system some of the features in temperature and salinity, are robustically incorporated. Thus, such hybrid models assimilate in a very simple way the data in the "sponge" layer to simulate the general circulation. They can be used also to study the sensitivity of the simulated currents to the change in temperature and salinity.

The analysis of model data shows that the quality of the results simulated in diagnostic model is not satisfying. However, free DW model is flexible enough to simulate such circulation which depart strongly from the circulation in diagnostic model, and agrees with some well known features of the Mediterranean Sea circulation. Generally, the simulated circulation is cyclonic. Due to the inflow of AW, surface currents in the Alboran Sea increase significantly, that results in substantial intensification of surface currents in the entire basin. With increasing depth a reversal of zonal flow is simulated. In the strait of Sicily, the transport at 156 m corresponds to the observed westward transport of LIW. The core of this transport is at about 300 m.

In the Ionian Sea, there is some qualitative similarity between currents in EDDC and ERPO. In the experiment ERHO, with homogeneous DW, deep currents are too different. This manifests that assuming homogeneous DW is very crude approach to remove physically inconsistent data. Model reconstruction of DW data seems to be preferable.

Acknowledgements

One of the authors was supported by the Alexander von Humboldt Foundation to carry out the numerical experiments in FRG. Thanks are due to V. Zalesni and to the reviewers for some useful remarks.

REFERENCES

Beckers J.-M. (1990). Application of the GHER 3D general circulation model to the Western Mediterranean. *J. mar. Syst.* (in press).

Bethoux J.-P. (1979). Budgets of the Mediterranean Sea. Their dependence on the local climate and on the characteristics of the Atlantic waters. *Oceanologica Acta*, **2**, 2, 157-163.

Bethoux J.-P. (1980). Mean water fluxes across section in the Mediterranean Sea, evaluated on the basis of water and salt budgets and of observed salinities. *Oceanologica Acta*, **3**, 1, 79-88.

Bryan K. (1969). A numerical method for studying the world ocean. *J. comp. Phys.*, **4**, 347-376.

Bryden H. L. and H. M. Stommel (1984). Limiting processes that determine basic features of the circulation in the Mediterranean Sea. *Oceanologica Acta*, **7**, 3, 289-296.

Farmer D. M. and L. Armi (1988). The flow of Atlantic water through the Strait of Gibraltar. *Prog. Oceanogr.*, **21**, 1-105.

Heburn G. W. (1989). Process studies of the circulation dynamics of the Western Mediterranean Sea, in: *Annales Geophysicae, Special Issue, XIV General Assembly of the European Geophysical Society, Barcelona*, 13-17 *March*, SII.1-6.

Hellerman S. and M. Rosenstein (1983). Normal monthly wind stress over the World Ocean with error estimates. *J. phys. Oceanogr.*, **17**, 158-163.

Holland W. R. (1975). Energetics of baroclinic oceans. In: *Proceedings Symposium on numerical models of ocean circulation, Durham, N. H. National Academy of Sciences, Washington, DC*, 168-180.

IOC/INF-772 (1989). Document préparatoire à l'élaboration du Programme de Recherche International en Méditerranée occidentale (PRIMO), 29 pp.

Lacombe H., J.-C. Gascard, J. Gonella and J.-P. Bethoux (1981). Response of the Mediterranean to the water and energy fluxes across its surface on seasoning and interannual scales. *Oceanologica Acta*, **4**, 2, 247-255.

La Violette P. (1985). The rationale for the Western Mediterranean Circulation Experiment, *WMCE Newslett.*, **4**, 1-4.

Levitus S. (1982). Climatological atlas of the world ocean. NOAA Prof. Paper. 13, US Government Printing office, Washington, DC, 173 pp.

Madec G., M. Chartier and M. Crepon (1989). Numerical simulation of deep water formation in the N. W. Med. Sea, in: *Annales Geophysicae, Special Issue, XIV^e General Assembly of the European Geophysical Society, Barcelona*, 13-17 *March*, SII.1-4a.

Malanotte-Rizzoli P. and A. Bergamasco (1989). The circulation of the Eastern Mediterranean Sea. *Oceanologica Acta*, **12**, 4, 335-351.

Malanotte-Rizzoli P. and A. Bergamasco (1990). The wind and thermally driven circulation of the eastern Mediterranean Sea. Part II: The baroclinic case. *Dynam. Atmos. Oceans* (in press).

Millot G. (1987). Circulation in the western Mediterranean Sea, *Oceanologica Acta*, **10**, 2, 143-149.

Nielsen I. N. (1912). Hydrography of the Mediterranean and adjacent water, *Rept. Dan. oceanogr. Exped. Medit.*, **1**, 77-192.

Ovchinnikov I. M., Y. A. Plakhin, L. V. Moscalenko, K. V. Negljad, A. S. Osadichii, A. F. Fedoseev, V. G. Krivosheja and K. V. Voitova (1976). *Hydrology of the Mediterranean Sea*, Hydrometeoizdat, Leningrad, 376 pp (in Russian).

Pacanowski R. C. and S. G. H. Philander (1981). Parameterization of vertical mixing in numerical models of tropical oceans. *J. phys. Oceanogr.*, **11**, 1443-1451.

Pinardi N and A. Navarra (1989). The seasonal and mesoscale variability of the Mediterranean: Primitive equation wind driven circulation studies. in: *Annales Geophysicae, Special Issue, XIV[e] Assembly of the European Geophysical Society, Barcelona,* 13-17 *March,* SII.1-1.

Plakhin Y. A. (1971). Formation of distinct deep water in the Mediterranean by convective mixing. *Oceanology,* **11**, 4, 524-52 .

Plakhin Y. A. (1972). Vertical winter circulation in the Mediterranean. *Oceanology,* **12**, 3, 344-350.

POEM Steering Committee (1985). POEM: A research program, Unesco. *Rept. mar. Sci.,* **35**.

Robinson A., R. A. Hecht, N. Pinardi, J. Bishop, W. G. Leslie, S. Rosentroub, A. Mariano and **S. Brenner** (1987). Small synoptic mesoscale eddies and energetic variability of the eastern Levantine basin. *Nature,* **327**, 6118, 131-134.

Sarkisyan A. S. (1975). The diagnostic calculations of a large-scale ocean circulation. in: *The Sea, Vol.* 6, John Wiley and Sons, New York, London, Sidney, Toronto, 363-458.

Sarkisyan A. S. and Y. L. Demin (1983). A semidiagnostic method of sea currents calculation. Tokyo, Japan, WCRP publication series. in: Large-scale oceanographic experiments in WCRP, 11, 1, 201-214.

Sarmiento J. L. and K. Bryan (1982). An ocean transport model for the North Atlantic. *J. geophys. Res.,* **87**, 394-408.

Schott G. (1915). Die Gewasser des Mittelmeeres. *Ann. d. Hydrogr. Marit. Meteor.,* **43**, 1, 2, 1-18, 49-79.

Semtner A. J. (1974). An oceanic general circulation model with bottom topography. Numerical simulations of weather and climate Technical Report N9, University of California, Los Angeles, 99 pp.

Stanev E. V. and H. J. Friedrich (1989). Numerical model of the general circulation in the Mediterranean Sea. in: *Annales Geophysicae, Special Issue, XIV[e] General Assembly of the European Geophysical Society, Barcelona,* 13-17 *March,* SII.1-2.

Stanev E. V., H. J. Friedrich and S. V. Botev (1989). On the seasonal response of intermediate and deep water to surface forcing in the Mediterranean Sea. *Oceanologica Acta,* **12**, 2, 141-149.

Takano K. (1974). A general circulation model for the world ocean. Numerical simulations of weather and climate, Technical Report N8, Department of Meteorology, University of California, Los Angeles, 47 pp.

Tziperman E. and A. Hecht (1988). Circulation in the eastern Levantine basin determined by inverse methods. *J. phys. Oceanogr.,* **18**, 506-518.

Wüst G. (1960). Die tiefenzirculation des Mittellandischen Meeres in den Kernshichten des Zwischen- und des Tiefenwassers. *Dt. hydrogr. Z.,* **13**, 3, 105-131.